TEM Image Analysis of Ceramic Nanoparticles Based on Machine Learning

Manoj Kautish[*]

LBEF Campus, Nepal

[*]*corresponding author*

Keywords: Machine Learning, Ceramic Nanoparticles, Transmission Electron Microscopy (TEM), Image Analysis

Abstract: With the current rapid development of China's national economy, the detection of ceramic defect materials and product quality risk assessment of ceramic material nano-casting products have gradually become an important link in the process of industrial quality production in China. In this paper, starting from the perspective of ceramic machine engineering learning, by designing and constructing a ceramic defect material polymerization classification recognizer, it can realize the automatic clustering of standard ceramic product material defects. The main content of the research and the focus of technological innovation are mainly divided into the following several main aspects: First, the production of a standard ceramic defect detection atlas. Second, feature extraction and selection. Finally, this paper studies and constructs an industrial defect sample cluster classification recognizer based on the ultra-micro machine deep learning classification clustering analysis algorithm, and performs classification clustering algorithm identification based on ceramic material sample classification defect samples. First, we analyzed the actual effect of the four types of defect characteristics on the actual effect of the identification of industrial defects based on the formation of ceramic material samples, and then started the analysis training verification experiment based on the classification and identification of industrial defects of ceramic material samples. From the ceramic standard sample defect recognition map, 180 ceramic standard sample defect recognition samples were selected and extracted, and the defect training set and analysis verification set were obtained by using the "leave out method" and the new layered contrast sampling method, and then through comparative analysis PCA clustering algorithm and analysis ReliefF algorithm. The ReliefF clustering algorithm in this paper shows that the analysis accuracy of the ceramic material sample classification defect sample cluster classification recognizer has reached 86.5%, and a good sample classification defect recognition experimental effect has been achieved.

1. Introduction

Ceramic materials, particles, nanotechnology, materials, particles, nanomaterials, ceramics, as an important solid ceramic material, have successfully obtained extensive micro-scientific theoretical research in our past decades. Due to the particularity of the micro-physical structure of this major ceramic material, in many stages of quantum technology theoretical research, we can only conduct in-depth research directly from the perspective of a major macro-physical structure, and it is difficult to directly conduct detailed research from a major micro-physical perspective. In-depth micro-science studies in simple terms, but a major macro-physical structure of a substance is often directly affected by the physical structure of a substance at the microscopic level. It is necessary to learn from the physical structure of the substance at the microscopic level. From the perspective of development, direct detailed, profound and simple research. With the continuous progress and development of modern quantum physics computer system simulation technology, the application of new quantum physics computer system simulation technology can also directly carry out the study of crystal growth. Quantum computing simulation technology theoretical research is practical in this respect from a new perspective. The above has also fully made up for the shortcomings of our previous theoretical research on quantum technology. Many foreign experts and scholars have studied this new technical development problem in a simple way from different technical theories, such as the development of self-dynamic technology theory of crystal grain growth, the development of statistical technology theory, and the technology of quantum physics topology. From the perspective of theoretical development, etc., a certain amount of research results had been successfully achieved. Therefore, by using a computer to automatically identify defects in the digital image of ceramic nanoparticles, it is possible to effectively overcome the misjudgment or missed judgment that often occurs in the current manual visual evaluation of films, and improve the effectiveness and accuracy of ceramic nanoparticle detection.

At present, for the identification of ceramic nano-particle defects, most of the domestic and foreign ceramic research institutes use manual visual inspection methods to detect the defect information in the image, and the efficiency is very low. However, the system based on traditional pattern recognition is mainly used to detect defects in small and local locations such as ceramic bonding, and is not suitable for the entire large-scale workpiece in railway ceramic nanoparticles, and it lacks universal adaptability. As the most researched subject at present, machine learning can continuously learn and improve its own performance characteristics through the use of data sets by computers to provide new ideas for the identification of ceramic nanoparticle defects, as well as for the automatic identification of ceramic nanoparticle defects.

Research progress in the analysis of ceramic nanoparticles based on machine learning in transmission electron microscopy: Ashour A proposed a deep learning-based deep-separable convolutional U-Net network architecture, using core-shell nanomaterials as the data set and using cross-entropy loss Function, and finally use the trained network to segment the TEM image and perform statistics to obtain structural information such as particle size and perimeter distribution, which provides the feasibility for the application of deep learning in the field of catalytic materials, but the research materials are still limited [1]. Bowman DT proposed a neuron segmentation algorithm based on active learning, which over-segmented neuron cell images into a certain number of superpixels, and then proposed a new query strategy to select the most representative from the unlabeled superpixel candidate set the super pixel subsets of sex and information content are marked and the pixels contained in them are marked. This method is not deeply involved in the analysis of ceramic materials [2]. Vangipuram R established a mathematical model of the particle

size distribution of the dispersed phase of nanocomposites based on fractal theory. This method is based on the sandbox method, which reduces the statistically significant influence on the evaluation parameters due to the small size of the nanocomposite TEM image, but the method is not sufficiently innovative in the development of this research [3]. Aiming at the common interface delamination failure problem in materials and structures whose three-dimensional dimensions are all at the nanometer level, Zou X uses focused ion beam technology (FIB) and transmission electron microscopy (TEM) to develop and design a set of research on the interface end of nanomaterials The experimental method of crack initiation behavior, but the research on the transmission electron microscope is not comprehensive [4]. Saray MT discloses a high-speed and high-resolution scanning microscopy imaging system and method based on machine learning. The light intensity distribution and corresponding Zernike polynomial coefficients of each distorted focus spot are input into the machine learning network for training to obtain a correction model, but the material performance Research is not very helpful [5]. Hwang PC uses image recognition technology to analyze different types of microstructure photos of steel materials under different conditions, and studies the influence of different image enhancement algorithms and machine learning algorithms on the recognition accuracy of steel microstructures, but it is obvious that the experiment The means of characterization is not microscopic enough [6]. Zhang Y N provides a transmission electron microscope (TEM) image interplanar distance measurement and analysis method based on deep learning and computer vision. Specifically, it includes two parts: deep learning part and computer vision processing part, but this method is of little significance to nano-level research [7].

This paper aims at the basic situation of the current domestic and foreign ceramic research institutes using manual visual inspection methods to detect the types and grades of defects in the radiographic images of ceramic nanoparticles. Defect characteristics research, feature extraction and selection, analysis of the weight ratio of each feature, and then use PAC data dimensionality reduction to test and analyze the defect feature data of ceramic samples, and finally get the optimized feature selection based on the PCA-ReliefF algorithm. The performance of clustering recognition of defects is trained mainly for pores, cracks and slag inclusion defects, and the generalization ability of the final recognizer is finally tested.

2. Principle and Overview

2.1. Overview of Machine Learning

As the core of modern artificial intelligence, the learning technology of robots is an innovative technology that enables human computer personnel to have a kind of automatic learning cognitive ability like robots. Now, it through in-depth research on how human computers can simulate or automatically realize various learning ability behaviors that affect humans to quickly acquire new learning knowledge or new skills, and redesign and organize the existing learning knowledge system structure and make it continuous Optimize and improve your own learning performance. Robot learning can usually be between several different technical theoretical disciplines. The main disciplines include basic computer science, statistics, mathematics and electronic engineering, etc., with a typical multi-disciplinary nature, a description of machine learning performance behavior in machine knowledge learning. Tom Mitchell from Carnegie Mellon University has repeatedly proposed that it is assumed that the P method of measuring performance is used to accurately evaluate the performance of a computer learning program in a certain category, the learning performance on T in the performance task. If a computer program makes a lot of performance improvements by making full use of the learning experience E to learn on T in this type of

performance task, then we can say that the performance of t and P is measured by P, and the program learns from experience E.

The main constraint optimization problem of the extreme learning machine is defined as the following formula

$$minLPELM = \frac{1}{2}\|\alpha\|^2 + C\frac{1}{2}\sum_{i=1}^{n}\|\gamma_i\|^2 \quad (1)$$

The constraints are

$$h(x_i)\alpha = t_i^T - \gamma_i^T, i = 1, \cdots\cdots n \quad (2)$$

In the equation: i=$[\gamma_i,1, \gamma_i,2, \cdots\cdots\gamma_i,q]$T is the vector error of the action collection of the sample xi by the q output nodes, and c is the regularization variable. According to the conditions of Kadoyili , the optimization problem encountered can be transformed into the following equation

$$\alpha = H^T\varphi, \varphi_i = C\gamma_I, h(x_i)\alpha - t_i^T + \gamma_i^T = 0, i = 1, \cdots\cdots n \quad (3)$$

Where: T is the Lagrange multiplier matrix. The final output weight α is calculated as the following formula

$$\alpha = H^T(I/C + HH^T)^{-1}T \quad (4)$$

Therefore, the output function of the extreme learning machine can be defined as the following formula

$$f(x_j) = h(x_i)H^T(I/C + HH^T)^{-1}T, j = 1, \cdots\cdots n \quad (5)$$

The extreme learning mechanism and the vector support principle are highly similar, you can convert the above kernel function into the extreme learning machine, and then limit the range of conditions for its function. The limit condition Merece theorem can transform the output into the following equation

$$f(x_j) = h(x_i)\alpha = [K(x_j, x_i) ... K(x_j, x_n)]^T(\frac{T}{C} + K)^{-1}T \quad (6)$$

In the equation: j = 1,..., n. After forwarding and simplifying processing, the program can classify and quantify the output of TEM images.

$$x(t) = 2\sum_{k=1}^{\frac{N}{2}-1} a_k\cos(kw_0t) + b_n\sin(kw_0t) \quad (7)$$

In the above formula:

$$a_k = C_K + \overrightarrow{C_K} \quad (8)$$

$$b_n = i(C_K + \overrightarrow{C_K}) \quad (9)$$

$$w_0 = \frac{2\pi}{N\Delta t} \quad (10)$$

Incorporating formula (7) into the dynamic balance differential equation, ignoring the effect of transient response, the following load excitation model can be obtained:

$$P(t) = (m_1 + m_2) + \sum_{k=1}^{\frac{N}{2}-1}[(m_1 + m_2)A_K - k^2w_0^2m_2P_2] \quad (11)$$

Machines, as learners' principle basis for classifying algorithms, are also diverse. According to

different learners' methods, that is, the difference in the size of different data centers and prior learning knowledge that different computers can handle, it can be roughly subdivided into There are 4 different types of wired supervised control learning, radio supervised control learning, semiconductor supervised control learning, and function-enhanced supervised learning. This paper focuses on unsupervised learning, as shown in Table 1:

Table 1. Specific content of unsupervised learning

	Classification/Regression	Structured learning	Reinforcement learning
Training data	(X,Y)	Structured (X, Y)	Training generation
Learning mode	f:X→Y	f:(X,Y)→ R	f:X→Y
Practical application	Multi-function calculation	Chinese-English translation	Playing games, image detection

One of the most widely used and most involved learning algorithms in machine learning is supervised learning. It needs to learn from training data first, and then classify unknown data. So supervised learning is actually designing a the best learning model under a certain criterion, it uses a set of labeled data training sample sets, and trains the parameters in the target classification function by continuously optimizing the cost function of the model, and finally obtains an optimal target simulation. The composite function realizes the correct division of the data in the training sample set. At the same time, the classifier generalizes its own ability through this "learning" method. When faced with unknown data, it also has the ability to correctly classify. Process [8-9]. Generally, the supervised classification ability learning model algorithm requires two training steps: the first step is one-time training, that is, by using a training sample set, first through the feature extraction and test selection of the thing model for a classifier, one is obtained. Input the data in the training matrix, and then use a training matrix data model and its feature flags to perform secondary training on the supervised classification processing capability model of a classifier to obtain a supervised classification capability learning algorithm model with higher accuracy and recognition rate the second step is the second test. The main method is to test the training sample set by using the same new set of feature-labeled data. After the same feature extraction and test selection, perform a second test on a classifier model obtained by training. In the second test, through the statistical analysis of the correct rate of the classification results, the learning ability of the classifier is examined, and finally the classification recognition performance of the classifier is continuously optimized through data feedback. Usual the basic flow of supervised learning algorithm is shown in Figure 1:
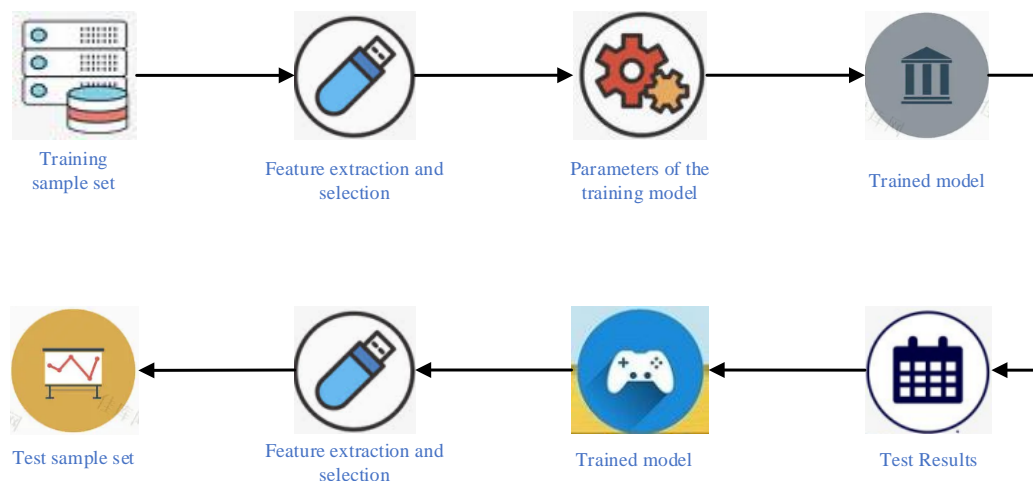
Figure 1. The general steps of supervised learning

2.2. Nanostructure of Ceramic Perovskite

Perovskite (perovskite) may have been officially named after Russia as the official English name of the famous German mineralogist Karl Perovski. It was used in 1935 as a commemoration of his first discovery in a scientific laboratory in 1839. The main material of calcium CaTiO3 mineral, it generally refers to a series of typical organic compounds with a large amount of calcium titanate and the same crystal structure as a large amount of CaTiO3 [10-11]. A typical perovskite crystal structure and its type are shown in Figure 2:
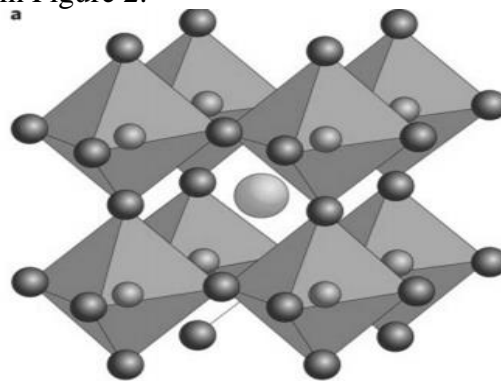

Figure 2. Schematic diagram of perovskite crystal structure

It is generally considered to have three points, namely the abx3 structure, where a and its b position and c and its b position are usually calcium and magnesium positive and negative hydrogen ions, and x positions are usually calcium negative and positive hydrogen ions respectively. One of the positive-negative hydrogen ions containing metallic calcium, because a and its b and c are negative-positive hydrogen ions, and c and c and x are combined through strong coordination bonds to form an octahedral metal ion coupling structure [bx6]4- , Points b and c are respectively located at the centers of the two upper halves of the octahedron, point x is located at the two center points and vertices of the octahedron, and one a and two positive and negative ions are considered to be It is directly filled in a crystal ion void formed by the octahedral three-dimensional metal ion bonding network [12-13].

Perovskite cubic crystals usually have a white metallic luster, and the main types of colors in the cubic crystals include gray black, brown, gray, orange, and some light metallic yellows. Although most of the organic compounds in perovskites are not considered to be oxides of organic salts or organic fluorides, they may also contain other chemically stable forms, such as halides, sulfides, and sulfides of organic salts. At present, the main chemical morphological stability of perovskite crystal structure is mainly composed of r and tolerance factor (t) in the tolerance qualitative and quantitative factors in the cubic crystal and the octahedral factor (µ) in the tolerance qualitative factor (µ) in the octahedron. It is decided that the chemical definition and calculation formulas of t in the tolerance qualitative and quantitative factors are:

$$t = \frac{R_A + R_X}{\sqrt{2}(R_B + R_X)} (12)$$

The octahedral factor µ is defined as:

$$\mu = \frac{R_B}{R_A} (13)$$

Perovskite or other organic compound materials similar to the perovskite functional structure are an important class of parent functional structural materials. At present, many of the parent functional structural materials discovered in new materials already have such functional structures, such as perovskite-like pressure Electrostrictive material element SrBi4-xLaxTiO15, magnetoresistive material (La,Ca)MnO3, resistance-induced stress-stretch functional material element Pb(Mg,Nb)O3, piezoelectric element Pb(Zr,Ti)O3, etc. Therefore, similar perovskite functional structure materials are a very important class of material matrix functional structures in a class of functional composite materials, and their main research results have important international scientific and technological significance and important economic application values [14-15].

Hybrid perovskite as a semiconductor processing material has been widely used in many applications such as organic optoelectronic devices and other photovoltaic power generation devices. Common ceramic nanoparticles mainly include zirconium dioxide, alumina, silicon dioxide, etc. This series of hybrid perovskites are divided into t and octahedral tolerance factor µ according to their tolerance inhibition factors, as shown in Figure 3:
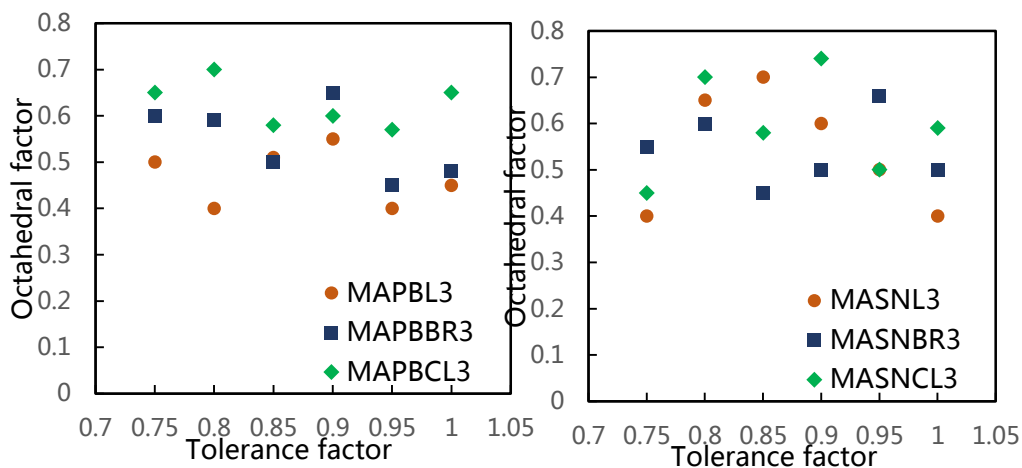

Figure 3. Tolerance factor values and octahedral factors of the structure of the halogen-organic-inorganic hybrid perovskite with different components

The crystal structure of perovskite undergoes a phase change with temperature changes. Taking $CH_3NH_3PbI_3$ as an example, the spatial lattice of ceramic nanostructures is shown in Figure 4:
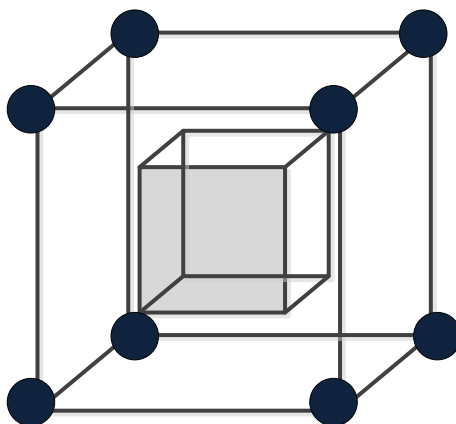

Figure 4. Schematic diagram of the crystal structure of perovskite at a certain temperature

2.3. Principle and Characterization of Transmission Electron Microscopy (TEM)

Transmission electron microscope (TEM), abbreviated as high-energy transmission electron microscope, uses the interaction of high-energy transmission electrons with the analysis sample, so that the high-energy electrons of the penetrated person and the sample can carry the electronic structure of the extracted analyst and the sample Physical information and sample component structure information, so as to obtain sample structure and microstructure analysis and testing methods. The main application of transmission electron microscopy is to accelerate the transmission of electrons by high-voltage microwaves, and obtain transmission electron waves with a transmission wavelength far or less than ordinary visible light, so as to obtain ultra-high resolution beyond traditional optical electron microscopes. Structure [16-17].

This paper uses a spherical aberration correction transmission electron microscope, the instrument model is FEI Titan-G. Titan-G2 spherical aberration correction electron microscope is a transmission electron microscope corrected by a convergent lens. It has a TEM/Scaning Transmission Electron Microscopy (STEM) mode, which can realize high-resolution imaging (HRTEM) and high-angle circular dark-field scanning transmission imaging (HAADF-STEM). At the same time, the supporting Super-X four-probe system can realize atomic-level energy spectrum (EDX) imaging. The main technical indicators are shown in Table 2:

Table 2. Main technical indicators of transmission electron microscope

Maximum magnification	1.5 million times (1500000X)
HAADF resolution	0.68A
HATEM resolution	0.8A
Accelerating voltage	High voltage 300KV
Spherical aberration corrector position	Condenser C2
Super-EDX function	Four probe system
Energy resolution of X-ray energy spectrometer	137 eV

(1) HRTEM principle and characterization

High resolution transmission electron microscopy (HRTEM or HREM for short) imaging is a contrast microscopy with phase difference, which can only accurately image most transmission crystal structure materials each atomic order of is arranged into an image. High or low resolutions imaging is a phase contrast phase, which is an interference transmission image directly formed due to the phase difference between all electron diffraction beams and interference transmission beams that can participate in transmission imaging. With the continuous development of various HRTEM imaging technologies and the continuous advancement of transmission electron microscopy itself, people have found that various HRTEM imaging can be used to directly observe the imaging of individual atomic arrays. One point that needs to be pointed out is that only the weak or strong phase body approximates and Only under the condition of Scherzer et al.'s under-focus requirement can a HRTEM atomic image taken by it reflect the crystal structure correctly, and at this time, it is difficult to meet the under-focus requirement of the weak or strong phase body approximation. When the phase thickness of some samples has exceeded a certain measured value, the approximate under-focus condition of the weak or strong phase body can only be completely invalidated. At this time, although there are still people who can directly shoot and get a clear crystal high-resolution image, it is not the phase contrast of HRTEM imaging and the transmission projection of the crystal structure are no longer closely related to each other [18-19].

(2) HAADF-STEM principle and characterization

Electrons interact with materials and generate different signals. The schematic diagram is shown in Figure 5. Among them, scanning transmission electron microscopy (scanning transmission electron microscopy, STEM) is to use a transmission electron beam with a very small convergent half-angle to perform transmission scanning up and down on a thin sample, and place different transmission on each sample. Receiver to facilitate the reception of different transmission signals for imaging. For example, when a ring-shaped transmission detector is placed under a thin sample to facilitate receiving a large amount of ring-shaped transmission neutral electrons scattered by low-angle sunlight, the transmission pixels formed by this sample are called a dark scene at a high angle or ring. Imaging (high-angle annular dark field scanning transmission electron microscopy, HAADF-STEM) [20-21]. Different from the HRTEM phase contrast image, the HAADF-STEM image is also called the atomic number contrast image (Z contrast image), and its contrast is proportional to the square of the atomic number Z.

(3) Principle and application of EDX energy spectrum

When an extranuclear electron beam is emitted from a sample to the surface of a sample shell, an extranuclear electron in the sample shell has a scattering effect on the electron beam emitted from the sample. The masses of the electrons outside the nucleus are equal, and almost all of them are inelastic scattering after they collide with each other. In the process of inelastic scattering of extranuclear electrons, most of the extranuclear energy lost in the incoming radioactive extranuclear electrons will be converted into extranuclear thermal energy. At this time, if an incoming radioactive extranuclear electron can have one Enough extranuclear energy will be injected into the outer layer of the inner shell of an atom [22-23]. For example, the outer layer of the atom k sends out the two outer nuclear emitting electron layers of the outer shell of the inner shell, while leaving a specific vacancy on the outer shell layer of the outer nuclear electron. At this time, the inner layer of the atomic shell an extranuclear emissive electron layer will jump up and move to this vacancy, thereby generating a characteristic X-ray (characteristic X-ray). Because different atomic elements with atomic characteristic number z can have different atomic ionization energy (Ec), the ionized nucleus of different atomic elements emits different electron characteristic number x radiation, and

the corresponding release of different elements is the specific data of X-ray is shown in Figure 6.
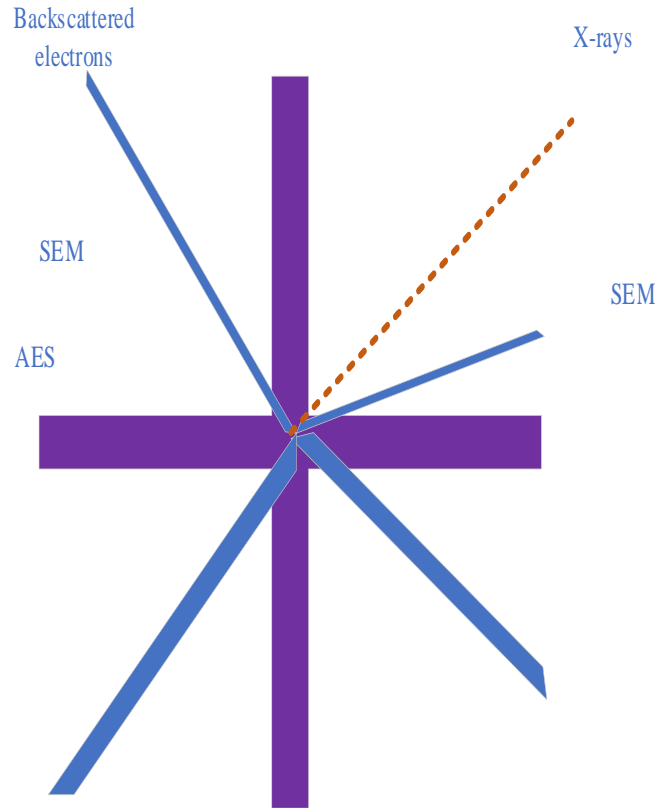

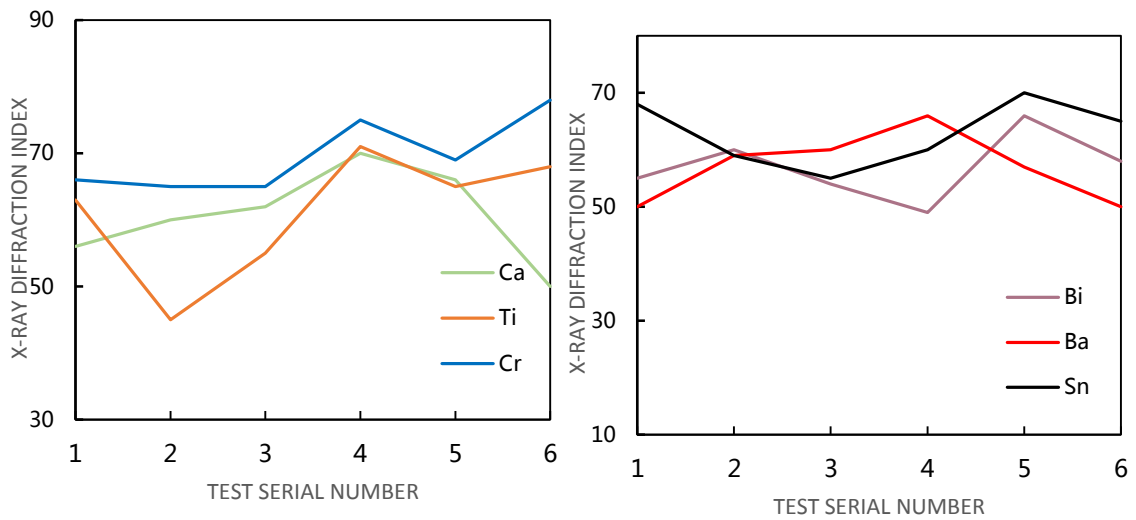*Figure 5. Schematic diagram of the interaction between electrons and materials*

Figure 6. The specific index values of X-ray released corresponding to different elements

3. Design Algorithm and Pattern Preparation

3.1. Machine Learning Algorithm

Different from the clustering criterion function based on the heuristic method, the clustering objective function is based on mathematical theory and objectively reflects the difference of things between classes and the similarity of things within classes. In this way, from a mathematical point of view, the clustering problem is transformed in order to find the optimization problem of the extreme value of the clustering objective function, the commonly used clustering objective function has the error sum of squares criterion and the weighted average square distance criterion. The error sum-of-squares criterion is the most commonly used clustering objective function. The main feature of the data sample object is that the data samples in each cluster that can be divided are dense and the number is not much different [24-25]. Then the error sum of squares criterion function formula is as follows:

$$J_C = \sum_{i=1}^{C} \sum_{x \in D_i} \|x - m\| (14)$$

Where C is the number of clusters to be obtained, and m is the average value of the samples in the i-th cluster D.

$$m = \frac{1}{n} \sum_{x \in D_i} x (15)$$

Where 1,2,...,i C and n_i are the number of samples in cluster Di. The error sum of squares criterion can be used to describe the total error sum of squares obtained when n data samples are clustered into C clusters. From formula (14), the value of the error sum of squares depends on the C clusters. The center average of the class. When the value of J_c is larger, the error is larger, and the effect of the corresponding clustering is also worse. Use this as the criterion to determine the smallest possible J_c, that is, the optimal cluster. result.

The weighted average square distance criterion is also a commonly used clustering objective function in cluster analysis. It is different from the characteristics of the data sample object to which the error sum of squares criterion applies. It can be based on the number of data samples in each cluster that the data sample object can be divided into. When the disparity is large, the formula of the weighted average square distance criterion is as follows:

$$J_1 = \sum_{i=1}^{C} P_i S_i^* (16)$$

Where C represents the total number of clusters of the clustering result, Pi is the prior probability and Si* represents the average squared distance between the data samples within the cluster.

$$P_i = \frac{n_i}{n} (17)$$

$$S_j(k) = w_j^d X_j(k-1) + \sum_i w_{ij}^I I_i(k) (18)$$

$$f(x) = \frac{1 - e^{-x}}{1 + e^{-x}} (19)$$

Where n represents the total number of data samples to be clustered, and ni represents the number of data samples divided into the i_{th} cluster.

$$S_i^* = \frac{2}{n_i(n_i - 1)} (20)$$

For the n data samples corresponding to the cluster Di, the combination between two is kind.

The evaluation of the generalization performance of the learner requires not only an effective and feasible experimental estimation method, but also an evaluation standard to measure the generalization ability of the model. In the field of machine learning, the confusion matrix is often used as an evaluation index for machine learning algorithm models to compare the performance of different models, so as to select the best learner that best meets the current learning task. Each column in the confusion matrix corresponds to the classification of the data sample obtained by the machine learning model, and each row in the confusion matrix represents the true classification of the data sample. The confusion matrix is generally a 2×2 matrix. Including real class (TP), false negative class (FN), false positive class (FP), true negative class (TN). Among them, Table 3 shows the parameters in the confusion matrix for the two-class model:

Table 3. Various evaluation indicators in the confusion matrix

Two-class confusion matrix		Real result	
		Positive	Negative class
Judgment result	Positive	Real class (TP)	False Positive (FP)
	Negative class	False negative class (FN)	True Negative (TN)

3.2. Preparation Method of Transmission Sample

In this experiment, Nanomill was used to further thin the cross-sectional transmission samples prepared by FIB. Unlike FIB's Ga ion source, Nanomill uses an Ar ion source. Under acceleration voltage, Ga ions will produce a relatively thick damage/amorphous layer on the surface of the sample, and ion implantation may occur, while low-energy Ar ion beams will not. Their similarity is that the higher the acceleration voltage, the thicker the damage layer produced. The ideal TEM sample is not only thin enough, but also not subject to any surface damage, and the roughness of the sample surface can be ignored. Although using FIB to thin the sample is one of the commonly used transmission sample preparation methods, the high-energy Ga ion bombardment used by FIB will cause damage or amorphization on the sample surface. Normally, FIB is used to thin the sample at 30kV. At this time, the thickness of the damaged layer on one side of the sample is greater than 30nm; at a low voltage of 5kV-10kV, the thickness of the damaged layer of the sample is about 5-10nm. The damaged layer will affect the TEM imaging and reduce the performance-to-noise ratio. The damage layer produced by the cross-sectional transmission sample prepared by FIB can be further cleaned by the low-energy Ar ion beam of Nanomill to reduce damage. The preparation process of the cross-sectional transmission sample of the perovskite solar cell is shown in Figure 7:
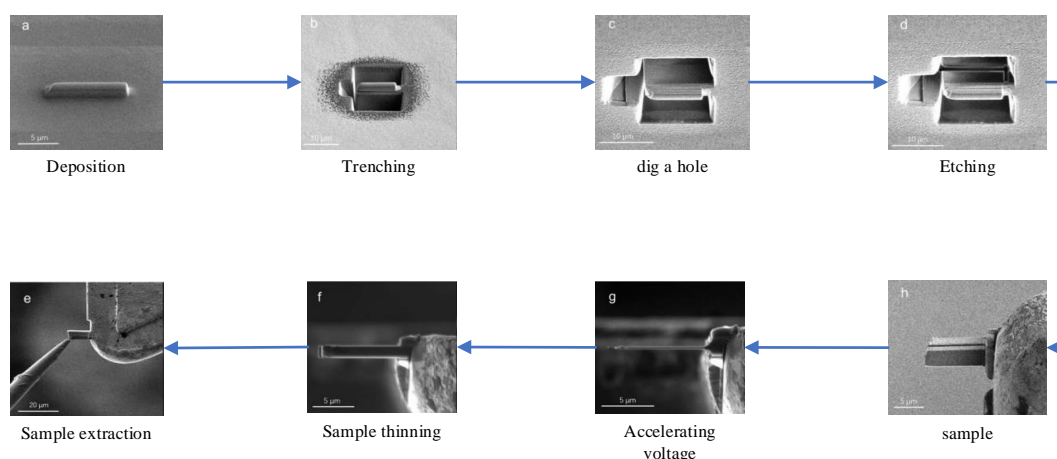
Figure 7. Flow chart of preparation of cross-sectional transmission sample of perovskite solar cell

TEM is one of the most intuitive analysis methods to characterize the microstructure of materials, and how to prepare ultra-thin samples that meet transmission electron microscopy analysis without damage or with low damage is a key step that restricts TEM analysis. Perovskite solar cells are thin-film materials with a multilayer structure and are extremely sensitive to temperature and humidity. They are easily degraded in humid and above room temperature environments, so it is difficult to use conventional mechanical polishing methods (requires Contact with water). First, a scanning electron microscope was used to irradiate the MA-type perovskite film with a voltage of 5kV and a current of 86pA. Figure 8 shows the SEM morphology changes of the MA-type perovskite film corresponding to the irradiated time of the MA type perovskite film.
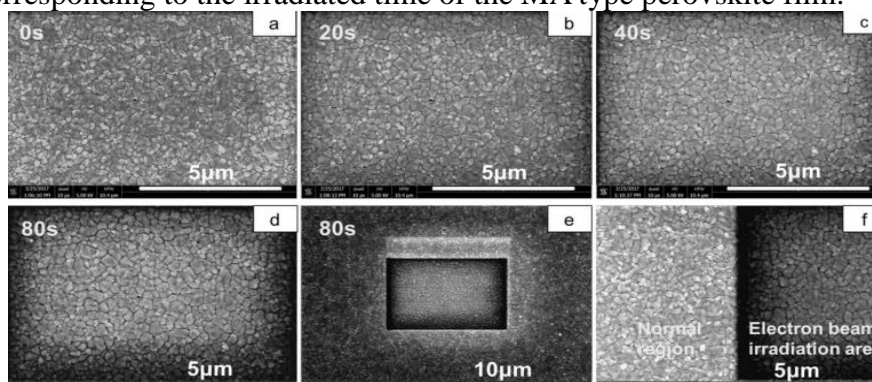

Figure 8. TEM morphology changes of MA-type perovskite film under different electron beam irradiation time

3.3. Machine Learning to Detect Important Parts of the Sample

Before radiographic inspection of bolsters and side frames, heat treatment, surface cleaning and appearance inspection must be carried out. Some ceramic samples with obvious defects and serious defects must be removed to improve the efficiency and value of radiographic inspection. For bolsters and side frames that are put into production for the first time, DR inspections should be performed on the important parts that are divided, namely A and B, and the manufacturer shall at least every quarter for the two bolsters and the A and B parts of the side frame. Perform DR detection. Among them, Table 4 is the highest level of allowable defects in each area of the side

frame, and for serious defects such as crack defects, not only are there no grades, but no part of the bolster or side frame is allowed to appear, otherwise it will be regarded as unqualified ceramics.

Table 4. The highest level of defects in each region of the side frame

Side frame defect level	AL area and AR area	BL zone and BR zone	Zone B1 and B4	Zone B2 and Zone B3
Stoma	Grade IV	Grade IV	Grade IV	Grade V
Slag and sand	Grade IV	Grade IV	Grade IV	Grade V
loose	Grade IV	Grade IV	Grade IV	Grade V

Whether it is the first batch of sampling or normal production or ceramic process change sampling, the laboratory needs to detect unqualified workpieces according to the requirements specified in Table 4, and analyze the causes of defects, take corresponding improvement measures, and re-sampling after improving the process, and inspect the ceramic products again until they meet the standards. By marking the minimum circumscribed rectangle of pore defects, crack defects and slag inclusion defects, the maximum coordinate value and minimum coordinate value of the rectangular boundary can be calculated, and the horizontal span and vertical span of the rectangle can be calculated from this. Since the orientation of the defect is in all directions, it is necessary to standardize the rectangular frame where the defect is located, that is, to achieve the unity of direction and length.

4. Experimental Results and Analysis

4.1. TEM Topography Analysis

In order to quantitatively characterize the effects of irradiation, we selected the SEM topography of the MA type perovskite after 10s, 60s, 120s, 180s, 240s, and 300s respectively, and selected three points in each image to measure it. The change of crack width at the grain boundary is summarized as shown in Figure 9:
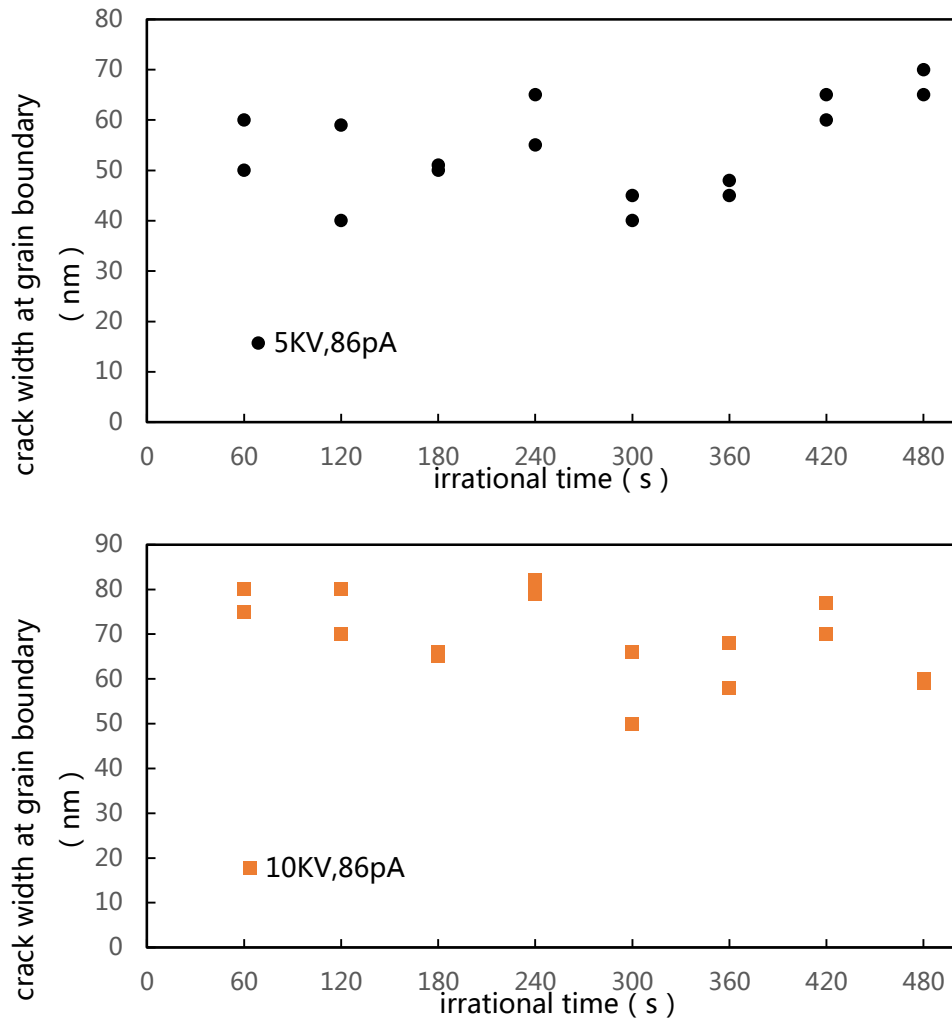
Figure 9. Variation of grain boundary crack width of MA-type perovskite film with irradiation time under different electron beam irradiation conditions

It can be seen from the figure that the image contrast is more complicated, not only the diffraction contrast formed by the difference in crystallographic orientation, but also the mass thickness contrast formed by the difference in the mass thickness value, so the specific shape of each sheet crystal cannot be observed. The electron diffraction pattern in this area has several crystal grains in a selected area of diffraction range, each has a different crystal orientation, and multiple sets of single crystal electron diffraction patterns overlap.

According to the electron diffraction analysis, the electron diffraction in the circular area is caused by the (101) crystal plane of ceramic ZrO_2. In the dark-field imaging mode, the beam deflector is used to adjust the incident angle of the electron beam, so that multiple adjacent 101 diffracted beams pass through the center of the objective lens, and at the same time, the objective diaphragm of the appropriate aperture is used to allow only the diffracted beams passing through the center of the objective lens to participate in imaging. According to the difference of image contrast, four crystals can be divided into I, II, III, and IV. The bright area corresponds to the crystal with strong diffraction excitation, and the dark area corresponds to the crystal with weak or no

diffraction. The image contrast shows that the ZrO2 crystal grains are of regular shape, stacked in hexagonal flakes, arranged tightly, the interface between the crystals is smooth and clear, the crystal size is relatively uniform, and the particle size ranges from 305 nm to 410 nm. Analysis by X-ray energy spectrometer shows that all particles in this area are composed of Zr and O elements, and no other metal elements are found. In the experiment, choose another area for the same central dark field imaging operation, and the morphological characteristics of adjacent grains can be clearly observed according to the difference of diffraction contrast.

4.2. Machine Learning Image Representation Analysis

Although the ReliefF algorithm can eliminate some irrelevant features that are not related to or have little effect on classification and recognition, it is limited to the existence of redundant features, while the PCA dimensionality reduction algorithm can effectively avoid the influence of redundant information and noise information. Then according to the ReliefF algorithm, each feature in the data sample (s-dimensional) is assigned corresponding feature weights, and finally the highest top few feature attributes corresponding to the feature weights that are most conducive to classification and recognition are selected to form the final feature subset (d dimension). In this paper, the performance of the ceramic sample defect clustering recognizer is used as the evaluation index, and the combination parameters s and d in the feature set are continuously trained to obtain the optimal feature subset, and finally the ceramic sample defect cluster recognition based on the optimal feature subset The machine algorithm's recognition rate of defects is shown in Figure 10:
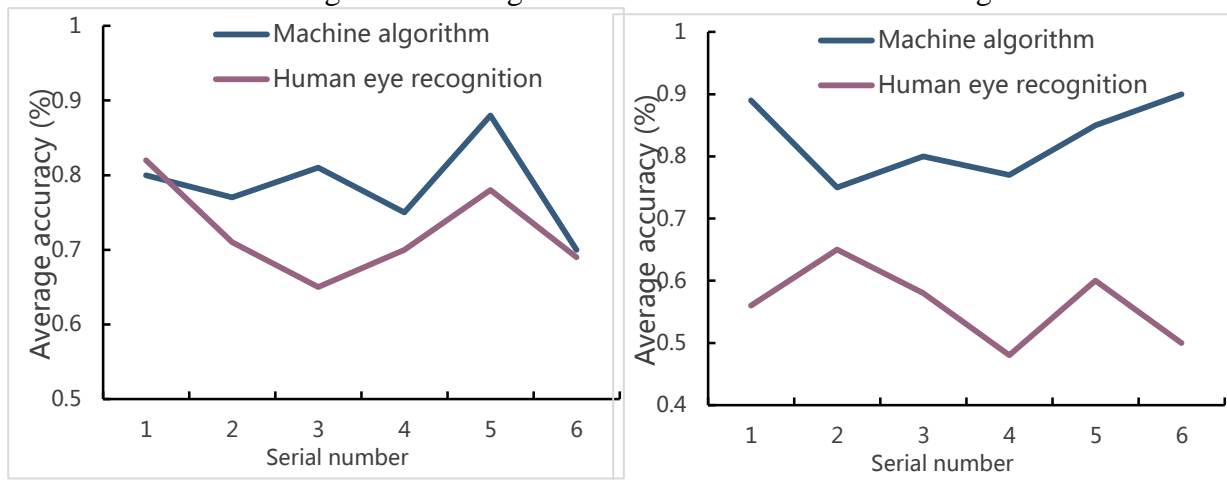

Figure 10. Analysis and comparison of TEM images based on machine algorithms and human eye recognition

From the data analysis in the figure, it is concluded that the basic shape features of the defects marked by the smallest circumscribed rectangle can better identify the crack defects, and there are a small number of identification confusions between the pore defects and the slag inclusion defects, and from the binary defect contour map the similarity of pore defects and slag inclusion defects can also be seen in the. The final accuracy rate of the clustering model also reached 88.3%, reflecting the effectiveness of these five basic morphological features for defect recognition, and conforming to the feature weight statistical data in ReliefF feature selection.

5. Conclusion

Ceramic nanomaterials meet the basic requirements of the development of various electronic industries in terms of quality, quantity and service, and create new opportunities and developments for the related equipment industry, material industry and instrumentation industry. In this paper, based on engineering machine language learning based on the extraction of TEM imaging images of ceramic material samples, the detection amount and research of the extraction defect types are constructed, and the defect type clustering negative film classifier is constructed to realize the automatic identification of various defects in the extracted ceramic material samples. The main content of the theoretical research and the focus of technological innovation in this paper are mainly believed to include the following main aspects: Research and make the defect clustering map in this standard. It is mainly aimed at extracting industrial TEM images of defective ceramic material samples in driver bolsters and train side frames in large passenger and freight passenger trains. Feature extraction and defect selection. In order for us to be able to better automatically detect and identify defect features in various ceramic products, the extraction diversity and recognition importance of defect features under different classification target sample tasks are analyzed. Construct a cluster classifier for ceramic defects. The defect performance of the sample defect performance aggregation classification recognizer based on the latest improved K-Means++ clustering algorithm is used as the main indicator of technical evaluation. This research paper is based on the recognition of various defects in TEM images in various ceramic material samples using machine deep learning. Although preliminary research has achieved some good results, this research paper will use machine deep learning technology to apply In the actual research and application process of clustering identification of defects in various ceramic material samples, there are still some key technical problems that have not been solved. Due to the limited working time and research energy, the paper still has some theoretical problems and technical limitations. , Needs further research and improvement.

Funding

This article is not supported by any foundation.

Data Availability

Data sharing is not applicable to this article as no new data were created or analysed in this study.

Conflict of Interest

The author states that this article has no conflict of interest.

References

[1] Ashour A , Obeidat K , Azrieh B , et al. An Association of Varicella Zoster Virus, Facial Palsy, and Meningitis in a Young Immunocompetent Male. Case Reports in Neurology, 2020, 12(1):136-139. https://doi.org/10.1159/000506192

[2] Bowman D T , Jobst K J , Helm P A , et al. Characterization of Polycyclic Aromatic Compounds in Commercial Pavement Sealcoat Products for Enhanced Source Apportionment.

Environmental Science and Technology, 2019, 53(6):3157-3165. https://doi.org/10.1021/acs.est.8b06779

[3] Vangipuram R , Nguyen H , Tyring S . What is the True Etiology of "Recurrent Shingles"?. SKIN The Journal of Cutaneous Medicine, 2021, 5(1):7-12. https://doi.org/10.25251/skin.5.1.2

[4] Zou X . Analysis of consumer online resale behavior measurement based on machine learning and BP neural network. Journal of Intelligent and Fuzzy Systems, 2021, 40(2):2121-2132. https://doi.org/10.3233/JIFS-189212

[5] Saray M T , Shahbazian-Yassar R . In Situ TEM Studies on the Nucleation and Growth of Multicomponent Alloy Nanoparticles on 2D Materials. Microscopy and Microanalysis, 2021, 27(S1):2978-2980.

[6] Hwang P C , Ku C Y , Chan C C . Detection of Malfunctioning Photovoltaic Modules Based on Machine Learning Algorithms. IEEE Access, 2021, PP(99):1-1.

[7] Zhang Y N . Can a Smartphone Diagnose Parkinson Disease? A Deep Neural Network Method and Telediagnosis System Implementation. Parkinsons Disease, 2017, 2017:1-11. https://doi.org/10.1155/2017/6209703

[8] Xu K , Wang Z , Zhou Z , et al. Design of industrial internet of things system based on machine learning and artificial intelligence technology. Journal of Intelligent and Fuzzy Systems, 2021, 40(2):2601-2611. https://doi.org/10.3233/JIFS-189252

[9] Ayyub K , Iqbal S , Nisar M W , et al. Stance detection using diverse feature sets based on machine learning techniques. Journal of Intelligent and Fuzzy Systems, 2021, 40(1):1-20. https://doi.org/10.3233/JIFS-202269

[10] Mingyu S , Jianjun W , Chenggao Y , et al. Study of Forecasting and Estimation Methodology of Oilfield Development Cost Based on Machine Learning. Chemistry and Technology of Fuels and Oils, 2021, 56(6):1000-1019.

[11] Vallejo-Huanga D , Ambuludi M , Morillo P . Empirical Exploration of Machine Learning Techniques for Detection of Anomalies Based on NIDS. IEEE Latin America Transactions, 2021, 19(5):772-779.

[12] Duan S R , Mirkov N S , Maleti S . Human Activity Recognition based on Machine Learning Classification of Smartwatch Accelerometer Dataset. FME Transactions, 2021, 49(1):225-232. https://doi.org/10.5937/fme2101225R

[13] He R , Weizhong M A , Ma X , et al. Modeling and optimizing for operation of C O 2 -EOR project based on machine learning methods and greedy algorithm. Energy Reports, 2021, 7(342):3664-3677.

[14] Yagnasri P , Seetharamaiah N , Sri P U . Magnetorheological Performance of Nano Magnetorheological (MR) Fluid Based on NiFe2O4 Nanoparticles. NanoWorld Journal, 2021, 7(1):1-7. https://doi.org/10.17756/nwj.2021-085

[15] Daniel C , Loganathan S . A Comparison of Machine Learning and Deep Learning Methods with Rule Based Features for Mixed Emotion Analysis. International Journal of Intelligent Engineering and Systems, 2021, 14(1):42-53.

[16] Nguyen P T . Application of Machine Learning in Construction Management. TEM Journal, 2021, 10(3):1385-1389. https://doi.org/10.18421/TEM103-48

[17] Golmohammadi D , Parast M M , Sanders N . The Impact of Service Failures on Firm Profitability: Integrating Machine Learning and Statistical Modeling. IEEE Transactions on Engineering Management, 2020, PP(99):1-15.

[18] Ponta L , Puliga G , Oneto L , et al. Identifying the Determinants of Innovation Capability With Machine Learning and Patents. IEEE Transactions on Engineering Management, 2020,

PP(99):1-11.

[19] Merham J , Rakowski A , Patterson J . Particle Picking in Cryo-TEM Images Using Machine Learning. Microscopy and Microanalysis, 2020, 26(S2):1-2.

[20] Tag H M , Saddiq A A , Alkinani M , et al. Biosynthesis of silver nanoparticles using Haloferax sp. NRS1: image analysis, characterization, in vitro thrombolysis and cytotoxicity. AMB Express, 2021, 11(1):1-12.

[21] Abebe B , Zereffa E A , Murthy H , et al. A novel poly (vinyl alcohol)-aided ZnO/Fe2O3 nanocomposite as an ascorbic acid sensor. Journal of Materials Science: Materials in Electronics, 2021, 32(6):7778-7790.

[22] Hay, Mon, Oo P , et al. Physicochemical characterization of forest and sugarcane leaf combustion's particulate matters using electron microscopy, EDS, XRD and TGA. Journal of Environmental Sciences, 2021, v.99(01):298-312. https://doi.org/10.1016/j.jes.2020.06.036

[23] Song X , Fu Y , Song C , et al. A special TEM Li-ion battery sample preparation and application technique for investigating the nano structural properties of the SEI in lithium ion batteries. MRS Advances, 2020, 5(27-28):1-7. https://doi.org/10.1557/adv.2020.262

[24] Zarei N , Behnajady M A . Optimization Of Photocatalytic Activity Of Mg/Zno Nanoparticles In The Removal Of A Model Contaminant Using Response Surface Methodology. Environmental engineering and management journal, 2019, 18(2):385-395. https://doi.org/10.30638/eemj.2019.036

[25] Kim S H , Kim S J , Shin H K , et al. Microstructural Analysis of Solder Bump Fabricated by Sn Electroplating on a PCB Substrate. Taehan-Kŭmsok-Hakhoe-chi = Journal of the Korean Institute of Metals and Materials, 2021, 59(4):233-238. https://doi.org/10.3365/KJMM.2021.59.4.233